Topological instability along invariant surfaces and pseudochaotic transport

G. M. Zaslavsky
Courant Institute of Mathematical Sciences, New York University, 251 Mercer Street, New York, New York 10012, USA and Department of Physics, New York University, 2–4 Washington Place, New York, New York 10003, USA

B. A. Carreras and V. E. Lynch
Oak Ridge National Laboratory, Oak Ridge, Tennessee 37831 USA

L. Garcia
University Carlos III, 28911 Leganes, Madrid, Spain

M. Edelman
Courant Institute of Mathematical Sciences, New York University, 251 Mercer Street, New York, New York 10012, USA
(Received 10 March 2005; published 31 August 2005)

The paper describes the complex topological structure of invariant surfaces that appears in a quasistationary regime of the tokamak plasma, and it considers in detail anomalous transport of particles along the invariant surfaces (isosurfaces) that have topological genus greater than 1. Such dynamics is pseudochaotic; i.e. it has a zero Lyapunov exponent. Simulations discover such surfaces in confined plasmas under a fairly low ratio of pressure to the magnetic field energy (β). The isosurfaces correspond to quasicoherent structures called "streamers," and the streamers are connected by filaments. We study distribution of time of particle separation, Poincaré recurrences of trajectories, and first time arrival to the system's edge. A model of a multibar-in-square billiard, introduced by Carreras *et al.* [Chaos **13**, 1175 (2003)] is studied with renormalization group method to obtain a distribution of the first time of particles arrival to the edge as a function of the number of bars, which appears to be power-like. The characteristic exponent of this distribution is discussed with respect to its dependence on the number of filaments that connect adjacent streamers.

DOI: 10.1103/PhysRevE.72.026227 PACS number(s): 05.45.Ac, 52.20.−j

I. INTRODUCTION

The goal of this paper is to give a detailed discussion of results for the so-called topological instability of particle dynamics that can appear in fluids and plasmas [1,2]. For any stationary vector field $\mathcal{A}(\mathbf{r})$ the field lines are solutions of the set of two equations that can be written in the form

$$\frac{dx}{\mathcal{A}_x} = \frac{dy}{\mathcal{A}_y} = \frac{dz}{\mathcal{A}_z} \tag{1}$$

if $\mathbf{r}=(x,y,z)$. The field $\mathcal{A}$ can be either the magnetic field $\mathbf{B}$ or the velocity field $\mathbf{v}$. Topological properties of $\mathcal{A}$ can be described through the topology of field lines.

It was known fairly long ago [3] that magnetic field lines can wind a surface $\mathcal{S}$ in the coordinate space and that the surface can be of a fairly complicated topology. The interest in the existence or nonexistence of magnetic surfaces $\mathcal{S}$ arose in the 1950s with respect to magnetic confinement of plasma by toroidal magnetic field configurations [4]. The papers of Tamm and Sakharov of that period were classified and unknown. Approximately at the same time, there was investigation of the magnetic surfaces by Ulam [5], who mentioned the connection of the problem of existence and stability of magnetic surfaces to the general problem of stability of dynamical systems.

In the following years the problem of magnetic surfaces appeared as an example of the problem of dynamical stability [6–8]. An important shift in the understanding of the problem of existence of magnetic surfaces was a link of these surfaces to invariant dynamical surfaces, so-called Kolmogorov-Arnold-Moser surfaces. Indeed, Eqs. (1) can be written as

$$\frac{dx}{dz} = \mathcal{A}_x/\mathcal{A}_z, \quad \frac{dy}{dz} = \mathcal{A}_y/\mathcal{A}_z. \tag{2}$$

These equations can be considered to be a dynamical system of 1 1/2 degrees of freedom with "time variable" z. Moreover, due to the condition div $\mathcal{A}=0$, which is valid for magnetic fields and for incompressible fluids, there exists a nonunique transformation

$$(x,y,z) \to (p,q,t) \tag{3}$$

and a function $\mathcal{H}(p,q,t)$ such that Eqs. (1) and (2) can be written in Hamiltonian form (see more, for example, in [9]). Then a magnetic surface when $\mathcal{A}=\mathbf{B}$ or a flux surface when $\mathcal{A}=\mathbf{v}$, if it exists, is the invariant surface of the corresponding dynamical system $(\mathcal{H};p,q,t)$.

The analogy of the field-line behavior in coordinate space and equivalent particle trajectories [Eq. (3)] allows the development of a theory of field-line chaos and the corresponding destruction of magnetic surfaces [10,11]. At the same time, simulations for the velocity field of a specific flow, known as Arnold-Beltrami-Childress flow, proposed by Arnold [12] and simulated by Hénon [13] show the existence of chaos of streamlines (see more in Ref. [9]). Later, this phe-

nomenon was named Lagrangian turbulence [14], and it comprised a more general situation because the Lagrangian particle satisfies the equation

$$\frac{d\mathbf{r}}{dt} = \mathbf{v}(\mathbf{r},t) \tag{4}$$

for a given velocity field $\mathbf{v}(\mathbf{r},t)$ that can be nonstationary. In the case that either $\mathcal{A}$ or $\mathbf{v}$ depends on time, the field lines do not exist by definition, and we will not consider such a situation. Because a charged particle in a strong magnetic field is "magnetized" and spirals along the magnetic field lines with very small Larmour radius, the magnetized charged dynamics is similar to the Lagrangian particle dynamics in zero-order approximation.

It is a common opinion, at least among physicists, that the integrability of dynamics is associated with the absence of chaos. The integrability is considered in the sense of the Liouville-Arnold theorem as a possibility to transform

$$\mathcal{H}(p_1,q_1;\ldots;p_N,q_N) \to \mathcal{H}(I_1,\ldots,I_N) \tag{5}$$

where $\mathcal{H}$ is a Hamiltonian of a system with N degrees of freedom (p_j,q_j), $j=1,\ldots,N$; I_j are N independent and commuting actions; and some other conditions applied [15]. Under these conditions, an integrable trajectory winds along the invariant surface, which is an N-dimensional torus. It was mentioned in Refs. [16,17] that the solution of the problem of integrability of a system depends on the meaning of "integrability." It was proved in Ref. [16] that the flux of geodesics along an invariant surface of the topological genus,

$$g(\mathcal{S}) > 1, \tag{6}$$

is not integrable. Some other conditions were mentioned that showed that existence of invariant surfaces wound by trajectories does not mean the integrability of the system in the Liouville sense (see review and references in Refs. [17,18]). In Ref. [19], the nonintegrability of trajectories in the square-in-square billiard due to the condition in Eq. (6) was discussed. The presence of N independent and commuting integrals of motion is not a sufficient condition for integrability [17–19]. In Ref. [1], a qualitative argument was given for why the transformation [Eq. (5)] cannot be time invariant for the invariant surfaces with $g(\mathcal{S})>1$. As a result, the trajectories are sensitive to small perturbations of initial conditions, and they possess randomness but not chaos. Moreover, for a simple example in [1], it was shown that the randomness of trajectories, despite the zero Lyapunov exponent, is sufficient to introduce a kinetic equation with fractional derivatives [20,21] in the description of particle transport in such systems.

Such random dynamics with a zero Lyapunov exponent is called "pseudochaos" [20,21]. It can happen in real systems that the main observable effects are due to the phenomenon of stickiness and to the sticky part of trajectories rather than to global dynamics. Such sticky dynamics can also be considered as pseudochaos because the corresponding Lyapunov exponent is negligible [22].

Although the fact of nonintegrability of dynamics with trajectories that wind filamented surfaces of nontrivial topology was known fairly long ago, there was not known, to our knowledge, any realistic system of this type until the paper [2]. Simulations of a typical three-dimensional example from plasma physics have displayed invariant isosurfaces $\mathcal{S}$ of constant velocity potential (stream function) with the topological genus $g(\mathcal{S})>1$. The paper [2] also provided a preliminary analysis and a billiard-type model to study the phenomenon of pseudochaos.

The present paper is a continuation of [2] with a detailed simulation of the physical model, detailed analysis of a simplified billiard-type model, and analytical studies of the models using the renormalization group approach. The structure of the paper is the following. In Sec. II we introduce some definitions and describe a connection between dynamics in billiards and pseudochaotic transport. This is an auxiliary section. In Sec. III we present results on simulations and visualization of the filamented invariant surfaces. Let us remark that in [2] we were able to show splitting of the invariant surfaces and emergence of filaments, while here the structure of the full isosurface and multiple filaments is shown explicitly. To our knowledge, it is the first explicit presentation of invariant surfaces with topological genus greater than 1 for a realistic model of confined plasma. It is worthwhile to comment that the existence of such isosurfaces leads to the necessity of a different concept of particle transport such as fractional kinetics of particles and their superdiffusion along the surfaces [1,23].

In Sec. IV we continue presentation of the results of plasma equation simulation and visualize various samples of passive particle trajectories along the filamented isosurfaces. These trajectories follow filaments and very closely reveal the trajectories in the multibar billiard system proposed as a model in [2]. The analogy is fairly strong up to filamentations of higher order that are not considered in this paper. The results of this section help to shape the multibar billiard model and to provide its analytical investigation in the following two sections. In Sec. V we construct the renormalization group equation for the Poincaré recurrences and with the solution of this equation we obtain the value of the transport exponent. A similar equation is obtained in Sec. VI where the exponent for the distribution of recurrences $\gamma(M)$ is a function of the number of bars M. We analytically obtain a power dependence of $\gamma(M)$ known before [2] from the simulation. We summarize the results in Sec. VII as a confirmation of the model proposed in [2] visualized numerically in this paper.

The notion of topological instability has two aspects: the appearance of filamented invariant isosurfaces with topological genus more than 1, and superdiffusive transport along these surfaces. This paper gives only numerical for the first aspect, while the second is studied in both numerical and analytical ways.

II. POLYGONAL BILLIARDS AND THEIR INVARIANT SURFACES IN PHASE SPACE

It is well known that for some special cases the behavior of dynamical systems can be modeled by the dynamics of a

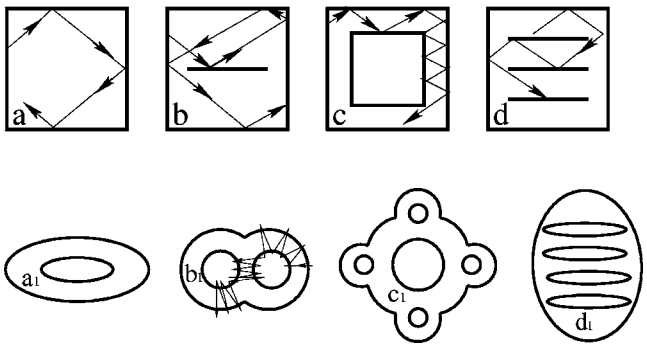

FIG. 1. Four examples of billiards and their corresponding invariant isosurfaces.

point particle in billiards with elastic collisions. This analogy is also important for our case. Consider a polygonal billiard, i.e., a billiard with angles at its M_0 vertices equal to $\pi m_i/n_i$, $i=1,\ldots,M_0$, where (m_i,n_i) are integers. Some rigorous results connecting the dynamics of polygonal billiards and flows along the corresponding surfaces in phase space can be found in Refs. [24,25]. Particularly, the topological genus $g(\mathcal{S})$ of the equivalent surface $\mathcal{S}$ is [24]

$$g(\mathcal{S}) = 1 + \frac{1}{2} n \sum_{i=1}^{M_0} \frac{m_i - 1}{n_i} \tag{7}$$

where n is the least common multiple of n_i. Equation (7) gives $g=2,5,4$ for the cases (b),(c),(d) in Fig. 1, where M is the number of bars in the square billiard table similar to Fig. 1(d). Then from Eq. (7)

$$g(\mathcal{S}) = 1 + M. \tag{8}$$

A result similar to Eq. (7) was presented in Ref. [19] where the square-in-square billiard [Fig. 1(c)] was considered.

There is a topological equivalence between the phase space structure for trajectories in billiards (a)–(d) and the surfaces $(a_1)-(d_1)$ of Fig. 1, but the geometric equivalence exists only for the rectangular billiard (a) and the torus (a_1). Therefore, the nonintegrability theorem of Kozlov [16,17], proven for the flow of geodesics, can be generalized for the billiard-type systems. The following is a simple qualitative consideration of nonintegrability for the cases shown in Fig. 1(b)–1(d). We consider a part of a trajectory that winds across a common part of the two "semitori" in Fig. 1(b). Approaching the point of bifurcation of the surface, the trajectory can wind along any of the split parts of the surface. In particular, this means that the transform [Eq. (5)] to the action variables $(I_1,\ldots,I_N)$ is not defined uniquely due to the bifurcation of the invariant surface [1]. Each filament of the surface has its own action (other comments can also be found in Ref. [19]).

Let ϑ be the angle of a trajectory with the horizontal axis in billiards (a) through (d) of Fig. 1. The trajectory is called rational if $\tan\vartheta = m/n$ is rational, and is called irrational if $\tan\vartheta$ is an irrational number. All rational trajectories are periodic and all irrational ones are ergodic and have Lyapunov exponent zero [24–26]. Nevertheless, the irrational trajectories have a weak mixing [27]; i.e., for almost all square integrable functions $G_1(x)$ and $G_2(x)$ (the x phase space coordinate of a particle in the billiard), the following limit is valid:

$$\lim_{t\to\infty} \frac{1}{t} \int_0^t dt[\langle G_1(x_t)G_2(x_0)\rangle - \langle G_1(x_0)\rangle\langle G_2(x_0)\rangle]^2 = 0, \tag{9}$$

where $\langle\cdots\rangle$ is averaging in phase space with natural measure [28]. Strong mixing, or simply mixing, means that

$$\lim_{t\to\infty}[\langle G_1(x_t)G_2(x_0)\rangle - \langle G_1(x_0)\rangle\langle G_2(x_0)\rangle] = 0. \tag{10}$$

Weak mixing can be accompanied by arbitrarily large and long-lasting fluctuations (i.e., deviations of the correlation function):

$$R(t) = \langle x(t)x(0)\rangle - \langle x\rangle^2. \tag{11}$$

The deviation from zero can be large and for a long time interval, but the time average of $R^2(t)$ is zero. Weak mixing dynamics is bursty and strongly intermittent [1,23].

III. DESCRIPTION OF A PHYSICAL MODEL

Let us consider a fluid model for a three-dimensional (3D) plasma in the toroidal geometry with a magnetic configuration characteristic of a tokamak system. In this model, the pressure gradient is the main plasma instability drive [29,30]. In plasmas, the pressure-gradient-driven instability is analogous to the Raleigh-Taylor instability in fluids when a layer of heavy fluid is over a layer of light fluid.

We will consider a description of the plasma dynamics based on a single-fluid approximation. In this framework, we consider the evolution of the plasma flows and pressure through a momentum balance equation and equation of state. These equations are coupled to the Maxwell equations. To simplify the system of equations, we make a further approximation. We assume that the aspect ratio of the torus, A, is large. Here $A=R/a$ where R is the major radius and a the minor radius of the torus. In the large A limit, one can neglect the fastest time scale of the system, compressional Alfvén waves, and the resulting set of equations is usually referred to as the reduced magnetohydrodynamic (MHD) equations [31]. We use this model to calculate the nonlinear evolution of the plasma. In this evolution, after a fast growth period, the plasma reaches a steady state. Depending on the strength of the pressure drive, the steady state is characterized either by the presence of turbulent flows or by a quasistationary flow. This transition between a laminar flow and a turbulent flow was studied in Refs. [2,32]. Here, we continue this investigation, and we present more detailed results characterizing the transport properties of the plasma under those conditions.

The underlying plasma instability for the different states is the so-called resistive pressure-gradient-driven instability that is present at the plasma edge [33], where the plasma has low temperature with moderate density levels, (i.e., it has high resistivity with finite pressure compared to the pressure of the magnetic field).

In writing these equations, we use the toroidal coordinate system (see Fig. 2): radius ρ, poloidal angle ϑ, and toroidal

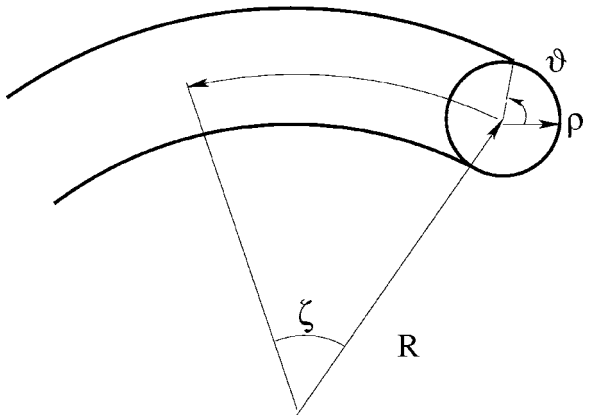

FIG. 2. Toroidal coordinates (ρ, ϑ, ζ).

angle ζ. We use the same notation as in Ref. [2]. Because of the assumption of a large aspect ratio, the plasma flow velocity is essentially perpendicular to the magnetic field and can be written as

$$\mathbf{V}_\perp = -\nabla\Phi \times \mathbf{B}, \tag{12}$$

where $\mathbf{B}$ is the magnetic field and Φ is the velocity stream function. The toroidal component of the vorticity U is given by

$$U = \frac{1}{B}\boldsymbol{\zeta}\cdot\nabla\times\mathbf{V}_\perp. \tag{13}$$

The parallel derivative operator $\nabla_\parallel$ in toroidal coordinates is

$$\mathbf{B}\cdot\nabla = \frac{B_\zeta}{R}\left(\frac{\partial}{\partial\zeta} - \frac{1}{q}\frac{\partial}{\partial\vartheta}\right), \tag{14}$$

where the so-called safety factor q is the poloidal rotational "frequency." Equations (12) and (13) allow us to express U in terms of Φ.

The dimensionless forms of the reduced MHD equations for the plasma, written in terms of U and pressure p, are [2]

$$\frac{dU}{dt} = -S^2\mathbf{B}\cdot\nabla\left(\frac{1}{\eta B_\zeta^2}\mathbf{B}\cdot\nabla\Phi\right) + S^2\frac{\beta_0}{\epsilon^2}\frac{\mathbf{b}(\mathbf{b}\cdot\nabla\mathbf{b})}{B}\cdot\nabla p + \mu\nabla_\perp^2 U,$$

$$\frac{dp}{dt} = D_\parallel\frac{R^2}{F}\mathbf{B}\cdot\nabla\left(\frac{R^2}{F}\mathbf{B}\cdot\nabla p\right) + D_\perp\nabla_\perp^2 P, \tag{15}$$

where η is the resistivity, $\mathbf{b}=\mathbf{B}/B$, $F=RB_\zeta$, $\beta_0 = p_0/(B_\zeta^2/2\mu_0)$ is the ratio of plasma pressure to the magnetic pressure, μ is the collisional viscosity, $D_\parallel$ and $D_\perp$ are diffusion constants with respect to the direction of $\mathbf{B}$, S is the Lundquist number, $\epsilon = 1/A$ is the inverse aspect ratio of the torus, and the convective derivative is

$$\frac{d}{dt} = \frac{\partial}{\partial t} + \mathbf{V}_\perp\cdot\nabla. \tag{16}$$

The numerical scheme, described in Ref. [2], is based on Fourier expansion in the poloidal ϑ and toroidal ζ angles:

$$\Phi = \sum_{m,n}\Phi_{m,n}(\rho,t)\sin(m\vartheta + n\zeta),$$

$$p = \sum_{m,n} p_{m,n}(\rho,t)\cos(m\vartheta + n\zeta). \tag{17}$$

We use finite differences for the discretization of the radial variable. The radial grid is nonuniform with 305 points; this gives a radial resolution of $r/a=0.002$ in the region $0.5 < r/a < 1$, where the pressure gradient drive is nonzero. The number of Fourier components used in the numerical calculations is 1700. In the numerical scheme, all linear terms in the equations are treated implicitly. The nonlinear terms are explicit. The time stepping is done in two substeps so that the scheme is second-order accurate.

To understand transport in this system, it is necessary to understand the structure of the flows. We use particle tracers to study them. The passive particle (tracer) dynamics is described by the equation

$$\frac{d\mathbf{r}}{dt} = \mathbf{V}_\perp(\mathbf{r},t). \tag{18}$$

Because of the form of the perpendicular velocity in terms of the stream function [Eq. (12)], the stream function is an effective Hamiltonian for the tracers. Therefore, when we refer to isosurfaces, we mean surfaces with a constant stream function Φ.

The structure of the isosurfaces is very complicated. Furthermore, because they wrap on a torus, their direct visualization is not necessarily helpful. To really visualize the three-dimensional structures, we have to unwrap them from the torus. To do so, we plot a Φ isosurface by first considering a single streamer in the $\zeta=0$ plane and following it along the torus. In the $\zeta=0$ plane, we draw a box around the streamer, and we extract the data from within the box. We do the same thing in each of the $\zeta=$const planes, but we change the size and shape of the box to fit in it the portion of the constant-Φ surface that is coming from the streamer that we selected in the $\zeta=0$ plane. The size of the box varies as we move around the torus. Therefore, the figure obtained by this method only provides information on the topology of the structure.

As discussed in Ref. [2], the solution of Eq. (15) depends critically on the value of the parameter β_0. For a fairly small value ($\beta_0=0.001$), there is a time relaxation of all Fourier components to a quasistationary regime with only the $n=25$ mode dominating the spectrum. Because of the toroidal geometry, each toroidal mode has many poloidal components with different m values. At higher β_0, several toroidal modes may compete for dominance, and the evolution shows a transition to a turbulent state.

Even in the case of a single dominant toroidal mode, the structure associated with it is quite complicated. In the outer region of the torus, the different poloidal components tend to reinforce themselves. they create eddy structures that are elongated in the radial direction (streamers) [34]. However, in the inner region of the torus, cancellations among the poloidal components result in multiple disjoint eddies. In 3D, the quasicoherent structures associated with these modes are

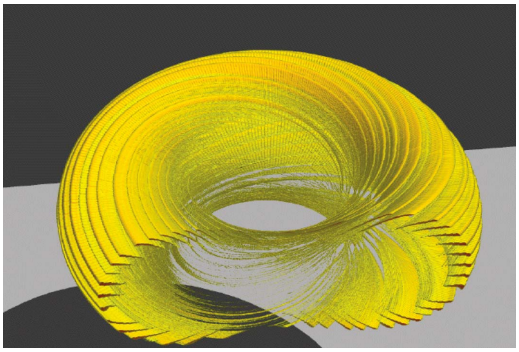

FIG. 3. (Color) Quasicoherent structures: Isosurfaces of interconnected streamers.

very complicated. Examples of such structures are shown in Figs. 3 and 4. All streamers are radially elongated and interconnected through filaments. A decomposition of each eddy (streamer) on a number of filaments is seen in Fig. 4 on the left half of the plate. More detailed views of selected isosurfaces are in Fig. 5 Part (a) shows one rotation around the torus; parts (b) through (d) are related to tracking twice around the torus. Each filament does not return to the same streamer. Instead, it does a twist and returns to another streamer. This behavior of filaments is not simple to visualize; even an oversimplified version for three filaments, shown in Fig. 6 for two different cases, is fairly complicated. Each thin channel or line in Fig. 6 corresponds to a filament that does not intersect others, and each thick line contour corresponds to a streamer. There are two different orders of filament-streamer connections in Fig. 6: (a) a simple connection with a twist and (b) the connection that corresponds to the so-called interval-exchange transformation that was discussed in Ref. [1] for the bar-in-square billiard in Fig. 1(b). In a realistic model (Fig. 5), several generations of filaments can be seen. In this paper, the calculations of the plasma turbulence have been carried out for a radial region that is twice the radial extension used in Ref. [2]. At the same time the number of Fourier components has been increased from 815 to 1700. This allows the formation of twice as many filaments for the invariant surfaces. Under these conditions, we carried out more detailed studies of the dynamics of particle tracers as will be discussed below.

To get some statistical properties of the particle tracers, we have implemented several diagnostics. One diagnostic is used to determine the trapping time distribution. It is based on the ϵ separation of trajectories [2,35,36]. When we start a particle tracer, we also initiate another one separated from the first by a radial separation $d(0)$. We follow both trajectories until they separate by a radial distance $d(\Delta t)$. The time Δt elapsed until they separate is the trapping time. The calculation is repeated many times to obtain a probability distribution of the trapping times. For the results presented here, we use $d(0)=0.001$ and $\epsilon=0.003$.

We have also measured the distribution of Poincaré recurrences. To do so, we start a cluster of tracer particles in a localized region in the plane $\zeta=0$. For each particle, we calculate the time required for it to come back to the region where it originated. From the time measurements, we calculate the probability distribution. For the results presented here, the region in the $\zeta=0$ plane is defined by $0.65<\rho<0.75$ and $-0.12<\theta<0.12$.

The following sections consider a model for particle dynamics along the filamented surfaces, theoretical analysis of the model, and comparison of the theory with simulation data.

IV. PARTICLE DYNAMICS AND TRANSPORT

The filaments in Fig. 5 have the shape of flat ribbons, which is a reason to consider a two-dimensional model of particle dynamics rather than a three-dimensional one.

In Ref. [2] a multibar-in-square (MBS) billiard model was proposed [see Fig. 1(d)], where the number of bars M is related in a simple way to the number of filaments. While this is an oversimplified model for topological construction of the isosurfaces, it can be considered a fairly good approximation because it follows from the simulation. The corresponding results are presented in Figs. 7 and 8. In Fig. 7, the trajectories of different particles colored in different ways are very close to the types of trajectories in the MBS model. Moreover, as shown in Fig. 8, where few trajectories have close initial conditions, separation of the trajectories is due to the specific topology of the filamented surface, and it is similar to the separation in the MBS billiard with a zero Lyapunov exponent. In fact, Figs. 7 and 8 show that there is

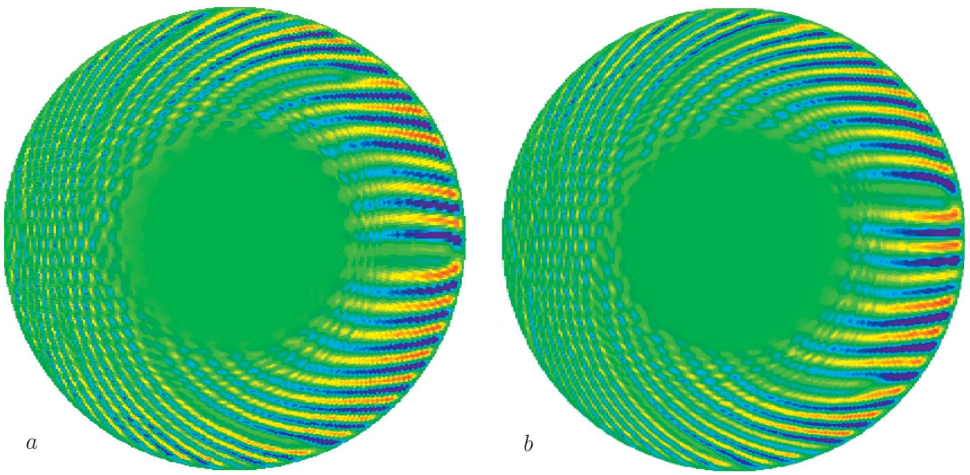

FIG. 4. (Color) Contours of sections of isosurfaces at two different poloidal planes. Colors show the magnitude of the stream function.

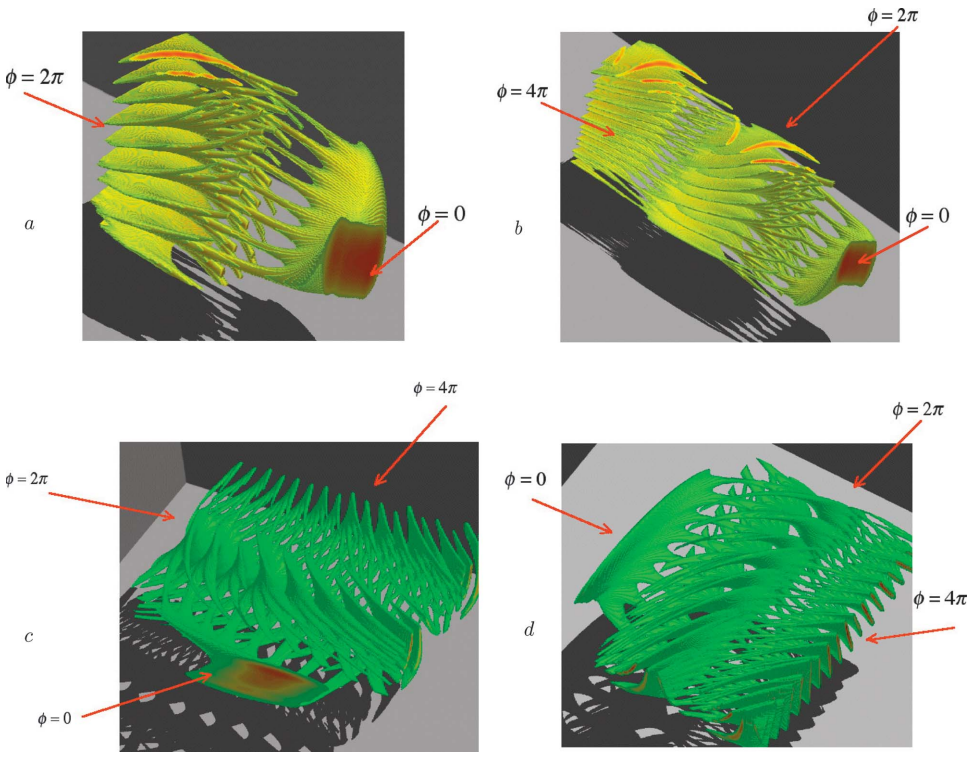

FIG. 5. (Color) Different views of an isosurface and its filamentation: (a) going once around the torus; (b)–(d) going twice around the torus.

some difference in the widths and lengths of filaments, and there can be several sets of filaments. Nevertheless, as a first approximation for the theory presented in the next sections, we neglect this difference and investigate a simplified model of MBS billiard with equidistant location of bars.

We need to make a further comment on the MBS model. The considered billiard-type model may be topologically equivalent to the model of particle dynamics along the isosurfaces presented in Fig. 5, but there is a metrical difference between topologically equivalent surfaces and real isosurfaces in the phase space of particles. The particle dynamics in Figs. 1(a)–1(d) has a zero Lyapunov exponent, and the dynamics in the billiards of Figs. 1(b) and 1(b)–1(d) is pseudochaotic [1,20]. The dynamics of particles along real isosurfaces in Fig. 5 can be characterized by a fairly small Lyapunov exponent (Λ). This means that the pseudochaotic MBS billiard model is only a good approximation for a fairly long time ($t_\Lambda \sim 1/\Lambda$).

Among the different ways to test the model, there is testing of the so-called ϵ separation of trajectories for small ϵ [2,35,36]. Let $d(t)$ be the distance between two trajectories with different initial conditions, and let $d(0) \ll R$ with R as a characteristic size of the system. We consider the condition

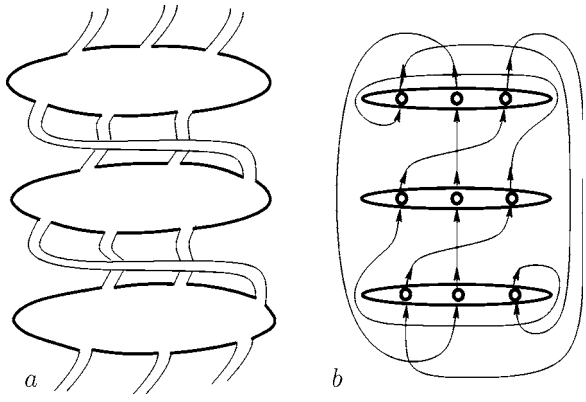

FIG. 6. A symbolic presentation of an isosurface with three streamers connected through the filaments. (a) Filaments connect the streamers with a twist; (b) each filament is a thin line with an arrow, and their connection with streamers is twisted by one connection point. This connection corresponds to the interval-exchange transformation.

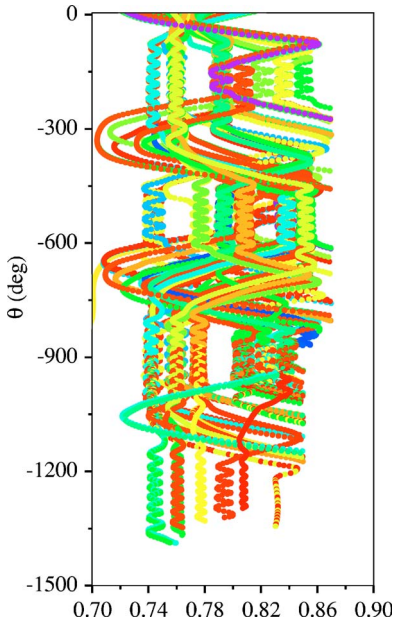

FIG. 7. (Color online) Tracer trajectories started at the same poloidal and toroidal angles but with different radii.

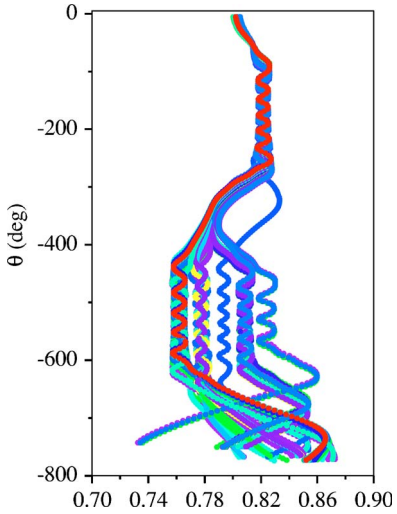

FIG. 8. (Color online) Dispersion of tracers along different filaments.

$$d(0) < d(\Delta t) = \epsilon \ll R \tag{19}$$

where Δt is a time of ϵ separation. For different initial pairs of trajectories, there will be different values for Δt, and one can consider the distribution function $P_\epsilon(\Delta t)$. This function is different from the probability distribution function (PDF) of Lyapunov exponents since for the definition of Λ one needs the condition $\epsilon \sim R$.

In the case of pseudochaos, $\Lambda = 0$ and dispersion of trajectories is polynomial, i.e.,

$$\ln d(\Delta t) = \ln \epsilon \sim \ln \Delta t + \text{const}, \tag{20}$$

and we expect a power law,

$$P_\epsilon(\Delta t) = \text{const}/(\Delta t)^{\gamma_\epsilon}, \tag{21}$$

where γ_ϵ is some constant exponent for large Δt. We call Δt the separation time and call $P_\epsilon(\Delta t)$ the PDF of separation time, or simply the distribution of separations.

To check the distribution of separations, we consider the tracer particle dynamics

$$\frac{d\mathbf{r}}{dt} = \mathbf{V}_\perp(\mathbf{r},t) + V_0\mathbf{b}, \tag{22}$$

where V_0 is the velocity along the magnetic field [compare to Eqs. (4) and (18)]. Because of the symmetry of the problem, the constant velocity V_0 can be arbitrary. In practice, it should be $V_0 \ll V_\perp$, otherwise many particles will never be influenced by the complicated structure of the velocity field $\mathbf{V}_\perp(\mathbf{r},t)$.

The results of the simulation are presented in Fig. 9. Particle trajectories stay very close while they travel in tubes of filaments, and they mix (weakly) in the streamers. The narrow tubes have an angular length poloidally of about π. This implies a length toroidally of $q\pi R$ where q is the so-called safety factor, or rotational number. From this, the maximum separation time is

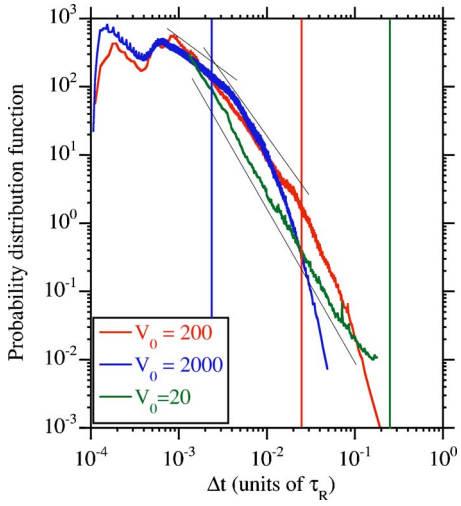

FIG. 9. (Color online) Distribution of separation time for different values of V_0 based on 50 000 initial pairs for each case, and $d(0)=0.001$, $\epsilon=0.003$.

$$\max \Delta t \sim q\pi R V_0. \tag{23}$$

As V_0 increases, the max Δt decreases and $P_\epsilon(\Delta t)$ exponentially decays due to randomly distributed initial conditions.

When V_0 is small or zero, the estimate (23) does not work and the random initial conditions play a different role because the mixing is defined by a random walk from one tube to another through the "free" space in streamers. Such a difference of trajectories is clearly seen from Fig. 10, where, assuming pseudochaotic particle behavior, one can expect a power law [Eq. (21)]. That is evident from Fig. 9 for $V_0 = 20$ with

$$\gamma_\epsilon = 2.18 \pm 0.2. \tag{24}$$

The calculations for this case were done with an initial separation $d(0)=0.001$ and for $\epsilon=0.003$. The statistics vary between 7 and 50×10^6 events, providing a very reliable result.

Returning to the model of a tracer that wanders along the streamers with filaments, we can consider the process of transport in a radial direction as the process of a random walk and the first arrival to the value $r \cong 1$. It is known that, in the case of a power law distribution and large t, the as-

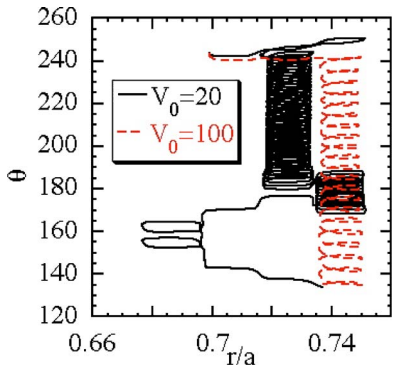

FIG. 10. (Color online) Samples of trajectories with different V_0.

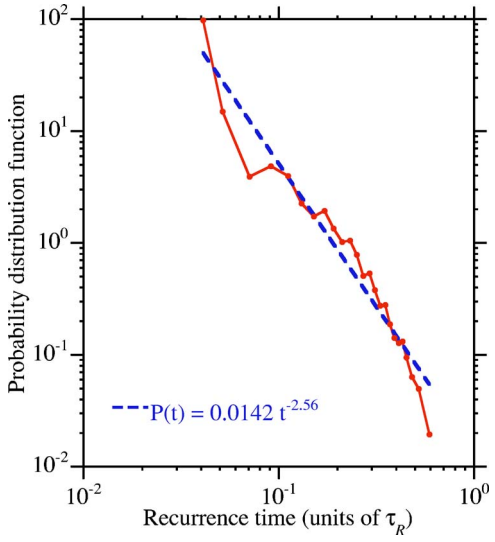

FIG. 11. (Color online) Distribution of Poincaré recurrences to the domain $0.65<r<0.75$; $-0.12<\nu<0.12$, $\zeta=0$. The statistics correspond to 38 878 events.

ymptotics of the PDF for the first arrival time is the same as the asymptotics for the PDF $P(t)$ of recurrences to a small domain in phase space at time t [23]. In turn, the asymptotics of $P(t)$ coincides with the PDF of separation $P_\epsilon(\Delta t)$ [37]. On this basis one can expect that

$$\gamma_\epsilon = \gamma_{\rm rec}, \tag{25}$$

where $\gamma_{\rm rec}$ is the exponent of $P(t)$. Although it is difficult to get good statistics for the PDF of recurrence time, the data in Fig. 11 are in fairly good agreement with Eq. (25).

V. DISTRIBUTION OF POINCARÉ RECURRENCES

For a tracer trajectory that starts in a small domain A of the phase volume Γ_A, the tracer dynamics is bounded. Due to that, the trajectory will repeatedly return to A infinitely many times. A time between two successive escapes from A is called a recurrence cycle. The probability density $P(t;A)$ of return to A with the duration t can be normalized by $\Gamma(A)$ if the phase space is uniform. Then the function

$$P(t) = \frac{1}{\Gamma(A)} P(t;A) \tag{26}$$

will be called the distribution of Poincaré recurrences, and it satisfies the normalization condition

$$\int_0^\infty P(t)dt = 1. \tag{27}$$

It was shown in Ref. [1] that, for an ensemble of irrational trajectories of the bar-in-square billiard [Fig. 1(b)], the cycles are discrete and their values t_n satisfy the scaling condition

$$t_n = \lambda_T^n g_T(n), \quad n \to \infty, \tag{28}$$

where n is a natural number, $g_T(n)$ is a slowly varying function of n, and for the scaling parameter λ_T,

$$\ln \lambda_T = \pi^2/12 \ln 2 = 1.186\ldots . \tag{29}$$

Using the diophantic approximation method we also showed that

$$P(t) = \text{const} \times t^{-\gamma}, \quad t \to \infty. \tag{30}$$

The recurrence exponent γ was obtained by simulation as

$$\gamma \approx 2.75. \tag{31}$$

In this section we show how the γ value can be obtained by using the renormalization group approach. The importance of having the function $P(t)$ is that Poincaré recurrence distribution can typically be linked to the transport properties of the considered system [23]. For example, a bar-in-square billiard that continues periodically in both the x and y directions (see Fig. 2 in [1]) has an infinite lattice of similar scatterers (bars in this case) and is known as a "Lorentz gas." The diffusion in this model is only along the y axis since there is conservation of the momentum along the x axis. It was speculated and confirmed numerically [1] that

$$\langle |y| \rangle \sim t^{\mu/2}, \quad t \to \infty, \tag{32}$$

where the transport exponent μ is given by

$$\mu = \gamma - 1 \sim 1.7 - 1.9; \tag{33}$$

i.e., by having the value of γ for Eq. (30) one can resolve the law of transport. The value $\gamma \approx 2.75$ was obtained in Ref. [1], while a more comprehensive simulation gives $\gamma \approx 2.8 \pm 0.1$. In fact, the result for γ slightly depends on the geometry of the billiard and on the selection of the ensemble of trajectories.

Let us introduce the probability $P_{\rm int}(t)$ to have the recurrence cycle time within the interval $(0,t)$. Then,

$$P_{\rm int}(t) = \int_0^t P(t)dt. \tag{34}$$

For the transition of t_n to t_{n+1} [see Eq. (28)], we assume that $P_{\rm int}(t_n)$ and $P_{\rm int}(t_{n+1})$ should be the same functions. This leads us to the renormalization group equation due to the specific property (28):

$$P_{\rm int}(t_{n+1}) = J_{n,n+1} P_{\rm int}(t_n) + \Delta P, \tag{35}$$

where ΔP plays the role of a boundary condition and does not follow the renormalization transform, and $J_{n,n+1}$ is a corresponding Jacobian. An important step is to consider a discrete set of time instants $(t_1, t_2, \ldots, t_n, \ldots)$ instead of the continuous time t.

Let ϑ be the angle of a trajectory with the x axis in the bar-in-square billiard. Then we can write

$$\tan \vartheta = a_0 + [a_1, a_2, \ldots], \tag{36}$$

where the continued fraction has been introduced:

$$\xi \equiv 1/[a_1 + 1/(a_2 + \ldots)] \equiv [a_1, a_2, \ldots],$$

$$\xi_n \equiv [a_1, \ldots, a_n] = p_n/q_n. \tag{37}$$

It is known [38] that the so-called Khinchin constant is given by [41]

$$\lim_{n\to\infty}(a_1 \ldots a_n)^{1/n} = 2.685 \ldots \equiv \lambda_a, \tag{38}$$

i.e., one can write

$$\prod_{k=1}^{n} a_k = \lambda_a^n g_a(n) \equiv \{a_n\}, \tag{39}$$

where $g_a(n)$ is a slow function of n.

Any statistical ensemble for the bar-in-square billiard or for the corresponding Lorentz gas consists of a large number of trajectories with different irrational $\tan\vartheta$. That means that the Jacobian in Eq. (35) can be presented in the form

$$J_{n,n+1} = \frac{dt_n}{dt_{n+1}} \frac{d\{a_n\}}{d\{a_{n+1}\}}. \tag{40}$$

The slowness of functions $g_T(n)$ in Eq. (28) and $g_a(n)$ in Eq. (39) means that

$$\lim_{n\to\infty} \frac{1}{n} \ln g_a(n) = \lim_{n\to\infty} \frac{1}{n} \ln g_T(n) = 0. \tag{41}$$

Using Eqs. (28), (39), and (41) we obtain

$$J_{n,n+1} = 1/(\lambda_T \lambda_a), \tag{42}$$

and the renormalization transform equation [Eq. (28)] occurs as

$$P_{\text{int}}(t_{n+1}) = \frac{1}{\lambda_T \lambda_a} P_{\text{int}}(t_{n+1}/\lambda_T) + \Delta P. \tag{43}$$

Equation (43) is a particular case of the general equation

$$f(t) = cf(t/b) + g(t). \tag{44}$$

The singular solution for Eq. (44) can be written as shown in Refs. [39,40]:

$$f(t) = t^{-\kappa}\left(K_0 + \sum_{\substack{n=-\infty \\ n\neq 0}}^{\infty} K_n \exp(2\pi i n \ln t/\ln b)\right), \tag{45}$$

where

$$\kappa = -\frac{\ln c}{\ln b} \tag{46}$$

and the sum provides the so-called log-periodic modulation of the main term with K_0. The leading term of this result, $f(t) \approx K_0 t^{-\kappa}$, can be obtained simply by its substitution in Eq. (44). It immediately gives Eq. (46). The constants K_n ($n = 0, 1, \ldots, \infty$) can be obtained by using the Mellin transform [40].

Comparing Eqs. (44) and (43), the expression (46) yields

$$\kappa = 1 + \ln \lambda_a/\ln \lambda_T = 1.83, \tag{47}$$

where the values of λ_T and λ_a, obtained from Eq. (29), are used. From the definitions [Eqs. (30) and (34)] we have

$$\kappa = \gamma - 1 = \mu, \tag{48}$$

which gives $\gamma = 2.83$, in good agreement with Eq. (31).

Let us comment that in [1,2] the relation (48) was considered on the basis of some qualitative speculations while here it is obtained from the renormalization group equation.

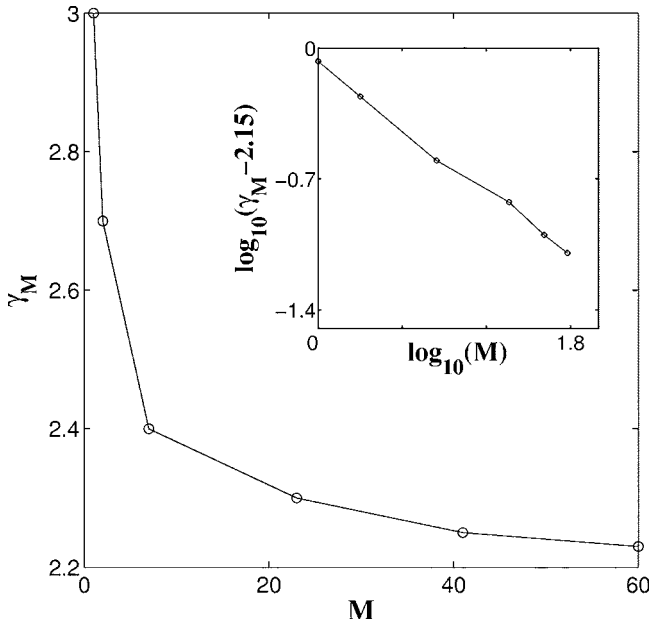

FIG. 12. Dependence of $\gamma(M)$ vs M obtained from 10^3 trajectories. Duration 10^8 each.

VI. MULTIBAR-IN-SQUARE BILLIARD MODEL

A multiplicity of bars is introduced as a model of an isosurface with filaments. Let $M \geqslant 1$ be the number of bars and the Poincaré recurrence distribution be

$$P(t;M) = \text{const}/t^{\gamma(M)}; \tag{49}$$

i.e., the recurrence exponent γ_M depends on M. In Fig. 12 we show this distribution, which can be presented in the form

$$\gamma(M) = \text{const}/M^{\delta} + \gamma_\infty, \tag{50}$$

where $\gamma_\infty = \gamma(M \to \infty)$. The result (50) is purely empirical. A similar result was obtained in [2], while the one in Fig. 12 is obtained with better statistics. Particularly, a more detailed simulation shows that $\delta \approx 0.6-0.8$ and

$$\gamma_\infty \approx 2.15 \tag{51}$$

(see Fig. 12). It was mentioned in Sec. III (see also [2]) that in the quasistationary regime only the $n=25$ mode dominates the spectrum. This number corresponds to the number of streamers in Fig. 4 and, for the billliard model, one can put $M=24$. For $M=24$, we have $\gamma(24) \approx 2.3$, which is consistent with γ_ϵ in Eq. (24) and with Eq. (25).

At the moment we cannot provide a complete theory of this result [Eq. (50)], but we can make some interpretation of it, based on the renormalization group approach.

The multibar billiard in Fig. 1(d) can be considered as a set of M similar one-bar billiards elongated along y with a distance 1 between bars. Let $P_A(t;M)dt$ be a probability to have a recurrence cycle t to a small domain A with phase volume $\Gamma(A)$ and M is the number of bars. Let us also take A

at the bar of the first billiard cell and consider $M \gg 1$. It is an important property of $P_A(t;M)$ that the limit exists

$$\lim_{M\to\infty} P_A(t;M) = P_A(t;\infty) \tag{52}$$

as follows from Fig. 12 and from Eq. (50).

We also assume that there exists a self-similarity of trajectories in phase space of any one-bar billiard cell. This property permits the following presentation:

$$P_A(t;M) \approx C[P_A(t;1)\Gamma(1)]^{M_0}, \tag{53}$$

where C is the normalization constant and $\Gamma(1)$ is the phase volume of the one-bar cell; i.e.,

$$\Gamma(1) = a\Delta(\cos\vartheta), \tag{54}$$

where a is the bar length and $\Delta(\cos\vartheta)$ is the interval of the velocities $\cos\vartheta$ for the ensemble of particles. The effective number $M_0 \leqslant M$ needs more discussion. Because of the existence of a limit [Eq. (52)] it is evident that the full number M of cells never works because the x and y coordinates for a one-bar billiard are within the interval $x \in (0,1)$, $y \in (0,1)$, while for the M-bar billiard $x \in (0,1)$, $y(0,M)$, and for any finite t and $M \to \infty$ the distant cells are seldom visited by trajectories that make input into $P_A(t;M)$. More accurately, considering the asymptotics $t \to \infty$, $M \to \infty$, we first perform the limit $M \to \infty$ and, second, the limit $t \to \infty$. For fairly large M we have $M_0 \ll M$ and we can estimate M_0 as

$$M_0 = \text{const} \times y_0(t;M), \tag{55}$$

where $y_0(t)$ is a characteristic coordinate along y for trajectories that make input into $P_A(t;M)$, and constant is related to the fixed ensemble width with respect to ϑ.

From Eq. (53) we obtain

$$\ln P_A(t;M) = M_0 \ln P_A(t;1) + C_1. \tag{56}$$

C_1 is an additional constant, or after substitution of Eqs. (49) and (55) into Eq. (56),

$$\gamma(M) = \text{const} \times y_0(t;M)\gamma(1) + C_1/\ln t. \tag{57}$$

Let us consider an integer ℓ:

$$1 \ll \ell \ll M_0 \ll M. \tag{58}$$

Similarly to Eq. (57), we have

$$\gamma(M/\ell) = \text{const} \times y_0(t;M/\ell)\gamma(1) + C_2/\ln t, \tag{59}$$

with a constant C_2, or

$$\gamma(M) = \frac{y_0(t;M)}{y_0(t;M/\ell)}\gamma(M/\ell) + \frac{C_2 y_0(t;M)}{y_0(t;M/\ell)\ln t} + \frac{C_1}{\ln t} + \gamma_\infty. \tag{60}$$

Equation (60) is similar to the renormalization group equation, where we need to estimate the transform coefficient:

$$J^{-1}_{M,\ell} = y_0(t;M/\ell)/y_0(t;M). \tag{61}$$

This can be done under the assumption of uniformity of scaling along y, and using the asymptotics of $\langle|y(t)|\rangle$ from Eq. (32) instead of $y_0(t)$:

$$J_{M,\ell} = t^{\mu/2}/(t\ell)^{\mu/2} = \ell^{-\mu/2}. \tag{62}$$

Substitution of Eq. (62) into Eq. (60) gives the equation

$$\gamma(M) = \ell^{-\mu/2}\gamma(M/\ell) + \frac{C_1 - C_2\ell^{-\mu/2}}{\ln t} + \gamma_\infty. \tag{63}$$

Equation (63) is of the form of Eq. (44) for large t, and the solution should be of the form of Eq. (45); i.e.,

$$\gamma(M) \sim \text{const}/M^{\kappa_\gamma} + \gamma_\infty, \tag{64}$$

where we left only the first term, and with

$$\kappa_\gamma = -\frac{\ln \ell^{-\mu/2}}{\ln \ell} = \mu/2 = \delta, \tag{65}$$

and δ is introduced in Eq. (50). Using the value of μ from Eq. (33) we have $\delta = 0.85-0.95$, which is slightly high compared to the values $\delta \approx 0.6-0.8$ from Fig. 12. The small difference can be explained by the approximations [Eqs. (59)–(62)] and by the level of accuracy for δ from simulations.

Finally for this section we should comment that for fairly large $M > 40$, the MBS billiard has the value of $\gamma_\infty \approx 2.2$, which is very close to the limit value $\gamma_c = 2$ when the mean recurrence time

$$\tau_{\text{rec}} = \langle t\rangle_{\text{rec}} = \int_0^\infty dt\, tP(t;M) \tag{66}$$

becomes infinite. This means that the MBS billiard almost never returns; i.e., a strongly nonequilibrium distribution of particles should be typical for such systems (see more in Ref. [21]).

VII. CONCLUSION

This paper pursues the following points.

(a) Simulations of resistive pressure-gradient-driven turbulence in plasmas show the existence of very complicated topology of invariant surfaces for the velocity potential. This topology has, in addition to streamers, elements called filaments. The topology of isosurfaces has genus $g(\mathcal{S})$ more than 1, providing a different view on the transport of particles along the isosurfaces. The value of $g(\mathcal{S})$ is closely related to the dominating ballooning mode.

(b) Particle dynamics along the isosurfaces is not integrable and can be modeled by the dynamics in multibar-in-square billiard. These dynamics are pseudochaotic; i.e., they are random but with a zero Lyapunov exponent.

(c) Despite a fairly rough approximate model of the description of particle dynamics along the isosurfaces, simulations show fairly good agreement between numerical results and the theory based on the renormalization group approach. The latter permits us to calculate all exponents related to the anomalous transport of particles.

(d) Pseudochaotic transport is relevant to systems with a zero or close-to-zero Lyapunov exponent. Anomalous properties of transport in such systems appear to represent a paradigm important to different applications in a number of dis-

ciplines, such as plasmas, condensed matter, and nonlinear optics.

ACKNOWLEDGMENTS

G.M.Z. and M.E. were supported by DOE Grant No. DE-FG02-92ER54184 and the Office of Naval Research Grant No. N00014-02-1-0056. This research is sponsored by the Direccion General de Investigacion (Spain) under Project No. FTN2003-08337-C04-01. Part of this research has been performed at Oak Ridge National Laboratory, managed by UT-Battelle, LLC, for the U.S. Department of Energy under Contract No. DE-AC05-00OR22725. G.M.Z. thanks V. Afraimovich, A. Neishtadt, and M. Shlesinger for many useful comments and valuable discussions. Simulation was suported by NERSC.

[1] G. M. Zaslavsky and M. Edelman, Chaos **11**, 295 (2001).
[2] B. A. Carreras, V. E. Lynch, L. Garcia, M. Edelman, and G. M. Zaslavsky, Chaos **13**, 1175 (2003).
[3] I. E. Tamm, *Fundamentals of the Theory of Electricity* (Gostekhizdat, Moscow, 1946) (in Russian).
[4] A. D. Sakharov, *Memoirs* (A. Knopf, New York, 1990), Chap. 9.
[5] S. M. Ulam, *A Collection of Mathematical Problems* (Interscience, London, 1960), p. 107.
[6] V. I. Arnold, Russ. Math. Surveys **18**, 85 (1963).
[7] V. K. Melnikov, Dokl. Akad. Nauk SSSR **148**, 1257 (1963).
[8] J. K. Moser, Mem. Am. Math. Soc. **81**, 1 (1968).
[9] G. M. Zaslavsky, R. Z. Sagdeev, D. A. Usikov, and A. A. Chernikov, *Weak Chaos and Quasiregular Patterns* (Cambridge University Press, Cambridge, U.K., 1991).
[10] M. N. Rosenbluth, R. Z. Sagdeev, J. B. Taylor, and G. M. Zaslavsky, Nucl. Fusion **6**, 297 (1966).
[11] N. N. Filonenko, R. Z. Sagdeev, and G. M. Zaslavsky, Nucl. Fusion **7**, 253 (1967).
[12] V. I. Arnold, C.R. Hebd. Seances Acad. Sci. **261**, 17 (1965).
[13] M. Henon, C.R. Seances Acad. Sci., Ser. A **262**, 312 (1966).
[14] H. Aref, J. Fluid Mech. **143**, 1 (1984).
[15] V. I. Arnold, *Mathematical Methods of Classical Mechanics* (Springer, Berlin, 1978).
[16] V. V. Kozlov, Dokl. Akad. Nauk SSSR **249**, 1299 (1979).
[17] V. V. Kozlov, *Symmetries, Topology, and Resonances in Hamiltonian Mechanics* (Springer, Berlin, 1996).
[18] V. I. Arnold, V. V. Kozlov, and A. I. Neishtadt, *Mathematical Aspects of Classical and Celestial Mechanics* (Springer, Berlin, 1987).
[19] P. J. Richens and M. V. Berry, Physica D **2**, 495 (1981).
[20] G. M. Zaslavsky and M. Edelman, in *Perspective and Problems in Nonlinear Science*, edited by E. Kaplan, J. E. Marsden, and K. R. Sreenivasan (Springer, New York, 2003), p. 421; Physica D **193**, 128 (2004).
[21] G. M. Zaslavsky and M. Edelman, Physica D **193**, 128 (2004).
[22] V. Afraimovich and G. M. Zaslavsky, in *Chaos, Kinetics, and Nonlinear Dynamics in Fluids and Plasmas*, edited by S. Benkadda and G. M. Zaslavsky (Springer, Berlin, 1998), p. 59.
[23] G. M. Zaslavsky, Phys. Rep. **371**, 461 (2002).
[24] E. Gutkin, Ergod. Theory Dyn. Syst. **4**, 569 (1984).
[25] E. Gutkin and N. Haydn, Ergod. Theory Dyn. Syst. **17**, 849 (1997).
[26] E. Gutkin, J. Stat. Phys. **83**, 7 (1996).
[27] E. Gutkin and A. Katok, in *Holomorphic Dynamics*, Lecture Notes in Mathematics Vol. 1345 (Springer, Berlin, 1989), p. 163.
[28] I. P. Cornfeld S. V. Fomin, and Ya. G. Sinai, *Ergodic Theory* (Springer, New York, 1982).
[29] J. P. Freidberg, *Ideal Magnetohydrodynamics* (Plenum, New York, 1987).
[30] H. P. Furth, M. N. Rosenbluth, and J. Killeen, Phys. Fluids **6**, 459 (1963).
[31] H. Strauss, Phys. Fluids **20**, 1354 (1977).
[32] L. Garcia, B. A. Carreras, and V. E. Lynch, Phys. Plasmas **9**, 47 (2002).
[33] B. A. Carreras, P. H. Diamond, M. Murakami, J. L. Dunlap, J. D. Bell, H. R. Hicks, J. A. Holmes, E. A. Lazarus, V. K. Pare, P. Similon, C. E. Thomas, and R. M. Wieland, Phys. Rev. Lett. **50**, 503 (1983).
[34] P. Beyer, S. Benkadda, X. Garbet, and P. H. Diamond, Phys. Rev. Lett. **85**, 4892 (2000).
[35] R. Bowen, Trans. Am. Math. Soc. **184**, 125 (1973).
[36] V. Afraimovich and G. M. Zaslavsky, Chaos **13**, 519 (2003).
[37] G. M. Zaslavsky and M. Edelman (unpublished).
[38] A. Ya. Khinchin, *Continued Fractions* (University of Chicago Press, Chicago, 1964).
[39] Th. Niemeijer and J. M. J. van Leeuwen, in *Phase Transition and Critical Phenomena*, edited by C. Domb and M. S. Green (Academic Press, London, 1976), Vol. 6, p. 425.
[40] B. D. Hughes, M. F. Shlesinger, and E. W. Montroll, Proc. Natl. Acad. Sci. U.S.A. **78**, 3287 (1981).
[41] E. W. Weisstein, http://mathworld.wolfram.com/KhinchinsConstant.html